Journal of Applied Polymer Science

Nanomechanical Mapping of Glass Fiber Reinforced Polymer Composites Using Atomic Force Acoustic Microscopy

Xilong Zhou,[1] Ji Fu,[1] Yingwei Li,[1] Faxin Li[1,2]

[1]State Key Lab for Turbulence and Complex Systems, College of Engineering, Peking University, Beijing 100871, China
[2]HEDPS, Center for Applied Physics and Technologies, Peking University, Beijing 100871, China
Correspondence to: F. Li (E-mail: lifaxin@pku.edu.cn)

ABSTRACT: In this work, a dual-frequency resonance tracking (DFRT) method was applied on atomic force acoustic microscopy (AFAM) and high-resolution, quantitative nanomechanical mapping of a glass fiber–reinforced polymer composites (GFRP) was realized. Results show that even using the single-frequency AFAM, the fiber, and epoxy can give very good contrast in amplitude images. The modulus mapping result on GFRP by DFRT AFAM was compared with that by dynamic nanoindentation, and it is found that DFRT AFAM can map the elastic modulus with high spatial resolution and more reliable results. The interface of GFRP was especially investigated using a 2 μm $\times$ 2 μm scanning area. Finite element analysis was implemented to investigate the effect of tip radius and the applied pressing force on the interface measurement using a sharp "interface". By setting a linear-modulus-varied interface with finite width in finite element analysis (FEA), similar comparison between FEA and AFAM experimental results was also implemented. The average interface width is determined to be 476 nm based on the high-resolution modulus image, indicating that AFAM is a powerful method for nanoscale interface characterization. © 2013 Wiley Periodicals, Inc. J. Appl. Polym. Sci. **2014**, *131*, 39800.

KEYWORDS: surfaces and interfaces; properties and characterization; theory and modeling

Received 12 March 2013; accepted 28 July 2013
DOI: 10.1002/app.39800

INTRODUCTION

Fiber reinforced polymer composites (FRP) is a large type of important structural materials widely used in aeronautic fields as well as in infrastructure engineering fields because of their high strength and light weight.[1–3] This kind of materials usually consists of two components, the fiber and the matrix, whose macroscopic mechanical properties differ much from each other. The interface is a small region between the fiber and the matrix ranging from tens of nanometers to several micrometers,[4,5] which is an important issue for FRP. During the manufacturing process, the fibers as well as the matrix are usually subjected to special treatments to enhance the composites' mechanical performance. Meanwhile, FRP are usually used under various ambient conditions, for example moisture, high temperature, prestress, etc., which may considerably affect or degrade the materials' performance.[6–8] The stiffness and strength of the interface are key factors affecting the load transfer between the fiber and the matrix and then the whole material's strength.[9,10] The interface can also be tailored to adjust the strength and fracture resistance to be a balanced status.[11,12] Besides, the failure of FRP usually initiates at the interface. Therefore, to better understand how the macroscopic mechanical properties evolve during the manufacture or duty process, it is crucial to characterize the micro/nanoscale mechanical properties of the interfaces, fibers, and matrix. To accomplish these missions, a quantitative, high-resolution as well as highly reliable characterization method is deeply required.

Many researchers have investigated the FRP as well as the interfaces using different characterization methods,[13–18] including nanoindentation (NI),[13–15] force-distance curves,[16] phase imaging,[16] transmission electron microscopy (TEM),[17] Raman spectroscopy,[18] etc. However, these methods suffer from more or less deficiencies in mechanical characterization of the composites especially the interface. NI, mainly used for single-point testing, is now the most widely used nanomechanical characterization method. While NI is inherently destructive because of its relatively large load (typically on the order of mN) and its lateral spatial resolution is limited by the indenter radius which is usually larger than 100 nm. The force–distance curve method based on atomic force microscopy (AFM) is only suitable for very soft materials. It has a poor resolution and is usually very time-consuming for array imaging. The TEM method can directly observe the interface

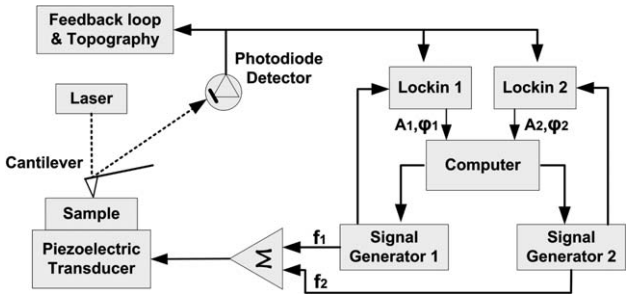

Figure 1. Schematic diagram of DFRT AFAM experimental setup.

structure and has a high spatial resolution but the sample's local mechanical properties cannot be obtained at all. The AFM phase imaging and Raman spectroscopy are useful and convenient methods for mechanical property mapping but quantitative interface characterization is generally difficult to realize.

Among all the above-mentioned methods, the AFM-based characterization methods should be more promising[19] as the tip radius of AFM cantilever is typically about 5–50 nm, which can give a very high lateral resolution and is thus very suitable for nanoscale characterization. The force applied by the AFM cantilever tip onto the sample ranges from tens of nN to several μN, which is much smaller than that in NI and nearly nondestructive for FRP because a large exerted force could induce plastic deformation on the epoxy matrix, making the elastic modulus measurements less accurate. Among all the AFM-based techniques, atomic force acoustic microscopy (AFAM) is a relatively new dynamic method very suitable for quantitative nanomechanical characterization.[20,21] Typically there are two imaging modes for AFAM. One is the single-frequency (SF) mode that gets the cantilever's amplitude and phase signals at a fixed excitation frequency. The SF AFAM can map the mechanically heterogeneous microstructures at nanoscale but quantitative information is generally difficult to achieve. The other is resonance-tracking (RT) AFAM, or contact resonance force microscopy (CR-FM), which tracks the contact-resonance frequency (CRF) at every pixel of the scanning area to get a CRF image. Using a reference material with known elastic properties, the modulus image can then be obtained based on a cantilever vibration model as well as a tip-sample contact mechanics model.[22] With a high lateral resolution as well as small applied force, AFAM is now probably the most suitable method for nanoscale mechanical property imaging of FRP, especially the small region near the interface. However, currently the AFAM with frequency sweep technique suffers from its low speed, which typically requires about 30 mins for a 256 × 256 pixels image.[23,24]

In this work, a dual-frequency resonance tracking (DFRT) technique was applied on AFAM and quantitative, high-resolution nanomechanical mapping of a glass fiber reinforced polymer composites (GFRP) was realized. Firstly, with both the SF AFAM and DFRT AFAM, the nanomechanical properties of a GFRP were systematically investigated. Modulus mapping by dynamic NI was also conducted to make a comparison with AFAM. Results showed that DFRT AFAM is a reliable method for high-resolution nanomechanical characterization. Finally, to precisely determine the width of the fiber/epoxy interface and show the high-resolution characterization of AFAM, interface mapping on a 2 μm × 2 μm scanning area was specially performed. Finite element analysis (FEA) was implemented to examine the effect of tip radius and applied force on interface measurement with a sharp "interface". By introducing a linear-modulus-varied interface with finite width in FEA, similar comparison between AFAM experimental results and FEA was also implemented. The average interface width was finally determined to be 476 nm based on 10 radial profiles randomly selected across the interface on the modulus image.

EXPERIMENTAL SETUP AND PRINCIPLE OF AFAM

In this section, we will briefly present the AFAM testing setup and the principle of resonance tracking AFAM to get the modulus mapping.

AFAM Testing Setup

Our AFAM testing setup is based on a commercial AFM (MFP-3D, Asylum Research, Santa Barbara, CA), as schematically shown in Figure 1. The cantilever tip contacts the sample surface with a constant pressing force. The testing sample is bonded tightly on a piezoelectric transducer so that it can vibrate synchronously with the transducer, which will further excite the cantilever's flexural vibration through the coupled tip-sample contact. The exciting signal to the piezoelectric transducer can be single-frequency or sweep frequency. In our experiment, a dual-frequency-resonance-tracking (DFRT) method was applied on AFAM to get the CRF at each pixel. The DFRT method is a fast and reliable feedback RT technique that uses two signal generators and two lock-in amplifiers. The principles and details of DFRT method can be found elsewhere[25] and will not be iterated here. The DFRT method had been successfully used in piezoresponse force microscopy,[25,26] whereas so far its application on AFAM are very few.[27]

Principle of AFAM

For AFAM quantitative measurement, the cantilever is usually modeled as an Euler–Bernoulli beam with a spring of k^* coupled to the sample surface representing the tip-sample contact stiffness, as illustrated in Figure 2. With the above beam model, the contact stiffness k^* can be expressed by the characteristic equation as[21]

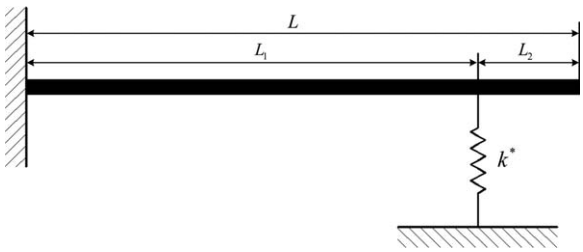

Figure 2. Euler–Bernoulli beam model for quantitative AFAM characterization.

$$\frac{k^*}{k_C}=\frac{2}{3}(\gamma\theta)^3\frac{1+\cos\gamma\cosh\gamma}{B} \quad (1)$$

where k_C is the spring constant of cantilever, $\theta = L_1/L$ is a tip location parameter, L is the whole length of the cantilever and L_1 is the length from the tip to the clamped end, $\gamma=\alpha_n L=\alpha_n^0 L\sqrt{f_n/f_n^0}$, α_n is the wave number of the nth flexural vibration of the surface coupled cantilever, f_n is the nth CRF, $f_n^0$is the nth free resonance frequency, $\alpha_n^0 L$ is the nth eigen-value of free flexural vibrations, with the first three roots to be$\{1.8751, 4.6941, 7.8548\}$, and

$$\begin{aligned}B=&[\sin(\gamma(1-\theta))\cosh(\gamma(1-\theta))-\cos(\gamma(1-\theta))\sinh(\gamma(1-\theta))][1-\cos(\gamma\theta)\cosh(\gamma\theta)]\\&-[\sin(\gamma\theta)\cosh(\gamma\theta)-\cos(\gamma\theta)\sinh(\gamma\theta)][1+\cos(\gamma(1-\theta))\cosh(\gamma(1-\theta))]\end{aligned} \quad (2)$$

The most common used contact mechanics model of the tip-sample contact is the Hertz contact model. In this model, the normal contact stiffness k^* is given by[28]

$$k^*=\sqrt[3]{6E^{*2}RF_N} \quad (3)$$

where R is the spherical tip's radius, F_N is the applied normal press force, E^* is the reduced elastic modulus of the tip-sample contact system, which can be expressed by

$$\frac{1}{E^*}=\frac{1}{M_t}+\frac{1}{M_s} \quad (4)$$

where M_s is the indentation modulus of the sample surface, M_t is the indentation modulus of the cantilever tip.

In practical measurement, the tip radius of curvature is usually difficult to determine, so a reference material with known modulus is required for calibration. Based on the CRF thus the contact stiffness data of the reference material, the reduced elastic modulus can be calculated,

$$E^*_{s-tip}=E^*_{ref-tip}\left(\frac{k^*_{s-tip}/k_C}{k^*_{ref-tip}/k_C}\right)^n \quad (5)$$

Where for a Hertz contact n=1.5, and for a flat punch contact n=1.0.[28]

Then the indentation modulus of the test sample can be calculated using the following equation:

$$M_s=\left\{\left(k^*_{ref}/k^*_s\right)^n\Big/M_r+\left[\left(k^*_{ref}/k^*_s\right)^n-1\right]\Big/M_t\right\}^{-1} \quad (6)$$

EXPERIMENTAL PROCEDURE AND FINITE ELEMENT ANALYSIS

Sample Preparation

The sample used in our experiments is a GFRPcomposites. The composites were prepared using a vacuum bag molding method to reduce the porosity. The shaped cylindrical bulk sample was then cut into wafers with the thickness of ~1 mm for testing. To reduce the influence of roughness on the CRF image, the samples were carefully grinded with alumina powder solution with the powder radius ranging from 20 to 1.5 μm and then carefully polished with 0.05 μm emulsion of diamond powder using a precision polishing machine. After polishing, the samples were then cleaned up using an ultrasonic cleaner to get rid of the small polishing particles on the surface.

Experimental Procedure

Before the AFAM testing, the measurement sensitivity to the spring constant of the cantilever was first examined in which three cantilevers with the spring constant of 48, 2, and 0.2 N/m were used. The forces applied on the tip were set to be 2 μN for the 48 N/m cantilever, 80 nN for the 2 N/m cantilever, and 10 nN for the 0.2 N/m cantilever, respectively, making the deflections of the three cantilevers to be approximately the same. The analysis results of CRF change as a function of modulus were shown in Figure 3 for both Hertz contact and punch contact, from which we can conclude that for soft material characterization <1 GPa, a probe with 0.2 N/m would be the best choice with small applied force; for materials whose modulus is less than 20 GPa, a probe with 2 N/m could be used; whereas for more stiffer materials, a probe with 48 N/m would be appropriate. As the modulus of the glass fiber is 60–90 GPa and the epoxy 3–6 GPa, a cantilever of 48 N/m should be chosen in our GFRP characterization. The spring constant of the cantilever used in our AFAM experiments is 41.85 N/m determined by a thermal calibration method.[29] Using this cantilever, we first conduct the SF AFAM testing, then the DFRT AFAM testing on the GFRP sample. As the NI is now a widely used tool for nanomechanical characterization and the dynamic NI can accomplish modulus mapping,[30] dynamic NI modulus mapping was also conducted on the GFRP sample to make a comparison with that by DFRT AFAM. Finally, the high-resolution interface characterization of GFRP was specially conducted within a 2 μm × 2 μm scanning area.

Finite Element Analysis

For the measurement of the fiber/epoxy interface width which is typically on the order of several hundred nm to several μm, as AFM always gives a larger size than the actual size because of the nonzero tip radius effect, it is necessary to specially investigate the effect of tip radius as well as the pressing force on the measured interface width. In this work, a 3-D finite element model (ABAQUS version 6.10.1) was employed to calculate the contact stiffness variations across a sharp fiber/epoxy interface (illustrated in Figure 4) as well as a linear-modulus-varied interface with finite width. In the calculation, all the materials used are set to be isotropic and linear elastic with Poisson's ratio of all materials to be 0.3 for simplicity. Young's modulus of the

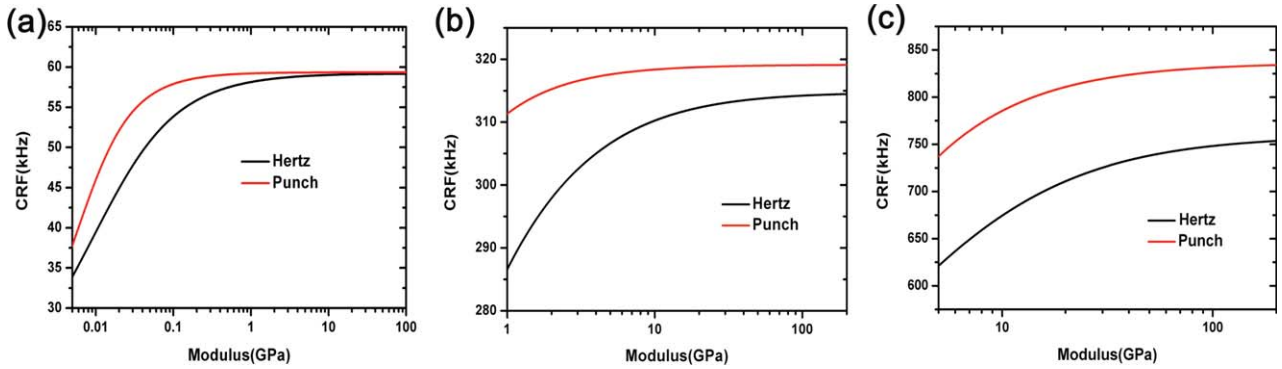

Figure 3. Sensitivity of the contact resonance frequency on the indentation modulus for cantilevers of different spring constants: (a) 0.2, (b) 2.0, and (c) 48 N/m, respectively, for both Hertz and punch contact. The applied force is 10 nN for the 0.2 N/m cantilever, 80 nN for the 2 N/m cantilever and 2 μN for the 48 N/m cantilever to make a constant deflection. The tip radius is set as 20 nm and the relative tip position $\theta = 0.98$. [Color figure can be viewed in the online issue, which is available at wileyonlinelibrary.com.]

silicon cantilever tip, the epoxy, and the fiber are 165, 5, and 65 GPa, respectively, based on the single-point NI measurement. The cantilever tip was modeled with four-node 3-D tetrahedron elements C3D4, which is very suitable for spherical body meshing and has a high accuracy after refinement. The epoxy as well as the fiber was modeled using eight-node 3-D hexahedron elements C3D8R, which has relatively high analysis accuracy and the analysis result is less affected when the mesh is highly distorted under contact condition. The dimensions of the FEA model were adopted that the longitudinal dimension along the symmetric plane is eight times larger than the tip radius and the dimension normal to the symmetric plane was six times larger than the tip radius. As to the depth (or thickness), it was set to be four times larger than the tip radius. Both the epoxy matrix and fiber were clamped at the bottom. The force–depth curve was obtained by setting a displacement loading and calculating the reaction force on the indenter tip. The contact stiffness can be approximately calculated by the following equation[31]:

$$k^i = \left.\frac{dF_N}{d\delta}\right|_{\delta=\delta^i} \approx \frac{1}{2}\left(\frac{F_N^{i+1}-F_N^i}{\delta^{i+1}-\delta^i} + \frac{F_N^i - F_N^{i-1}}{\delta^i - \delta^{i-1}}\right) \quad (7)$$

Here k^i is the contact stiffness of the ith load step, F_N^i and δ^i is the magnitude of the normal applied load and the corresponding deformation of the ith load step, respectively. To investigate the effects of tip radius on the contact stiffness, a series of radii of 25, 50, and 100 nm are used. The applied displacement on the tip was set to be 3 nm with the increment of 0.03 nm to make the large-deformation analysis stable and accurate. With the help of the FEA simulation results, the contact stiffness variations across a sharp "interface" and a linear-modulus-varied interface with finite width can be evaluated, which would help us to determine the interface width in practical measurements.

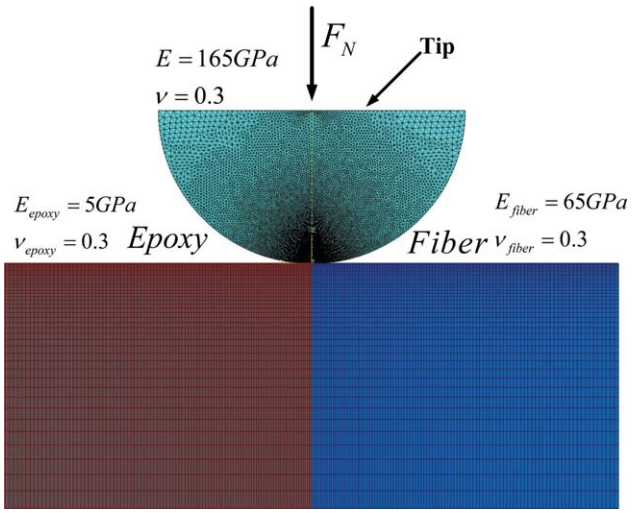

Figure 4. Schematic of finite element model for the contact stiffness variation calculation between the AFM tip and epoxy (left)/fiber (right). [Color figure can be viewed in the online issue, which is available at wileyonlinelibrary.com.]

RESULTS AND DISCUSSION

Qualitative Nanomechanical Imaging by Single-Frequency AFAM

Figure 5 shows the images of a GFRP (18 μm × 18 μm) obtained using the single-frequency (SF) AFAM. Figure 5(a) is the topography image in which the round fiber and the epoxy matrix can be clearly observed with height difference up to about 80 nm in the scanning area. The topography image is obtained in contact mode by keeping the cantilever's average static deflection constant during the whole scanning process. Figure 5(a) shows that the fiber is slightly lower than the epoxy matrix. This is probably because of the fact that during compression polishing, the surface may be strictly flat, whereas after removing the compressing force, the epoxy will expand much more than the fiber because of the larger difference in modulus. Previous studies[20,32,33] have shown that large height change or topography roughness could influence the CRF of the cantilever tip-sample configuration. Thus an accurate and reliable modulus measurement requires the sample surface be strictly flat. However, in most cases, this ideal condition is very difficult to be satisfied for composite. Note that the fiber and epoxy were very flat in their own region and the height changes gradually

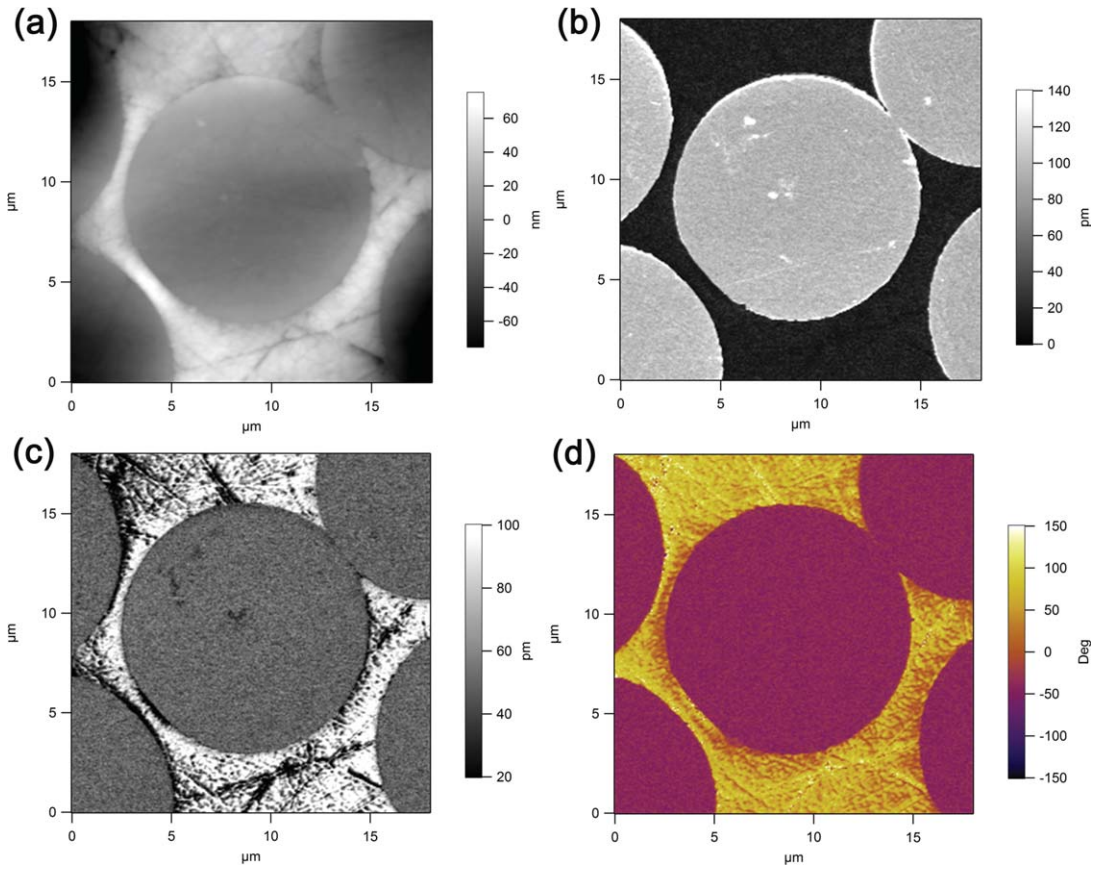

Figure 5. Single-frequency AFAM images of a GFRP: (a) topography; and (b), (c) the amplitude images obtained at the excitation frequency of 712.93 and 630.36 kHz, respectively; and (d) the phase image. [Color figure can be viewed in the online issue, which is available at wileyonlinelibrary.com.]

across the interface [Figure 5(a)], so in the following quantitative characterization the effect of topography roughness on the CRF image was just ignored and thus the calculated modulus image.

Figure 5(b,c) are the amplitude images by SF AFAM obtained at 712.93 and 630.36 kHz, respectively, which both give distinct contrast between the fiber and epoxy but show contrast inversion at these two excitation frequencies. In SF AFAM mode, sometimes the contrast inversion can even appear in only one single amplitude image if the CRF shift is larger than the half-width of the resonant peak.[20] Because of the contrast inversion problem, even qualitative mechanical characterization is somewhat difficult with SF AFAM. That is, from Figure 5(b,c), one cannot tell whether the bright or the dark region is stiffer, unless we know in advance that the fiber is much stiffer than the epoxy. Figure 5(d) shows the phase image obtained at 630.36 kHz. At both sides of the contact resonance peak, the phase images are similar and did not show contrast inversion. Note that here the phase contrast should be related to CRF shift during scanning at different positions. The phase signal shifted according to the CRF shift, thus phase contrast emerges. Meanwhile, from the amplitude images and phase image, the interface between the fiber and epoxy can be clearly distinguished although the exact width is difficult to measure because of the large scanning range.

Quantitative Modulus Mapping by DFRT AFAM and Dynamic NI

For quantitative nanomechanical characterization, DFRT AFAM on the same scan area was conducted, as shown in Figure 6. Using the DFRT technique, the scan speed can reach up to 2 Hz while to prevent the cantilever from quick damage, the scan speed was set at 0.5 Hz for all testing which means a 256 × 256 image requires about 8 mins, much faster than that of about 30 mins using the frequency sweep AFAM.[32] Figure 6(a) is the CRF image of the GFRP. It can be seen that the epoxy and the fiber have a CRF difference of about 80 kHz, indicating that the CRF is very sensitive to the modulus difference. With the CRF data of the testing sample, the indentation modulus can be calculated using aforementioned eqs. (1–6) with a reference material whose elastic property is known by other methods. Figure 6(b) shows the indentation modulus image calculated using a fused silica (indentation modulus of 75 GPa) as the reference material and the Hertz contact model. Figure 6(c) is the modulus distribution of the indicated line in Figure 6(b), from which we calculated that the indentation modulus is 59.3±6.02GPa for the fiber with the relative error about 10.15% and that of 4.63±0.72GPa for the epoxy with the relatively error about 15.55%. From Figure 6(a,b), it can also be seen that AFAM is sensitive to scratches, because the contact area significantly changed between tip and sample surface.

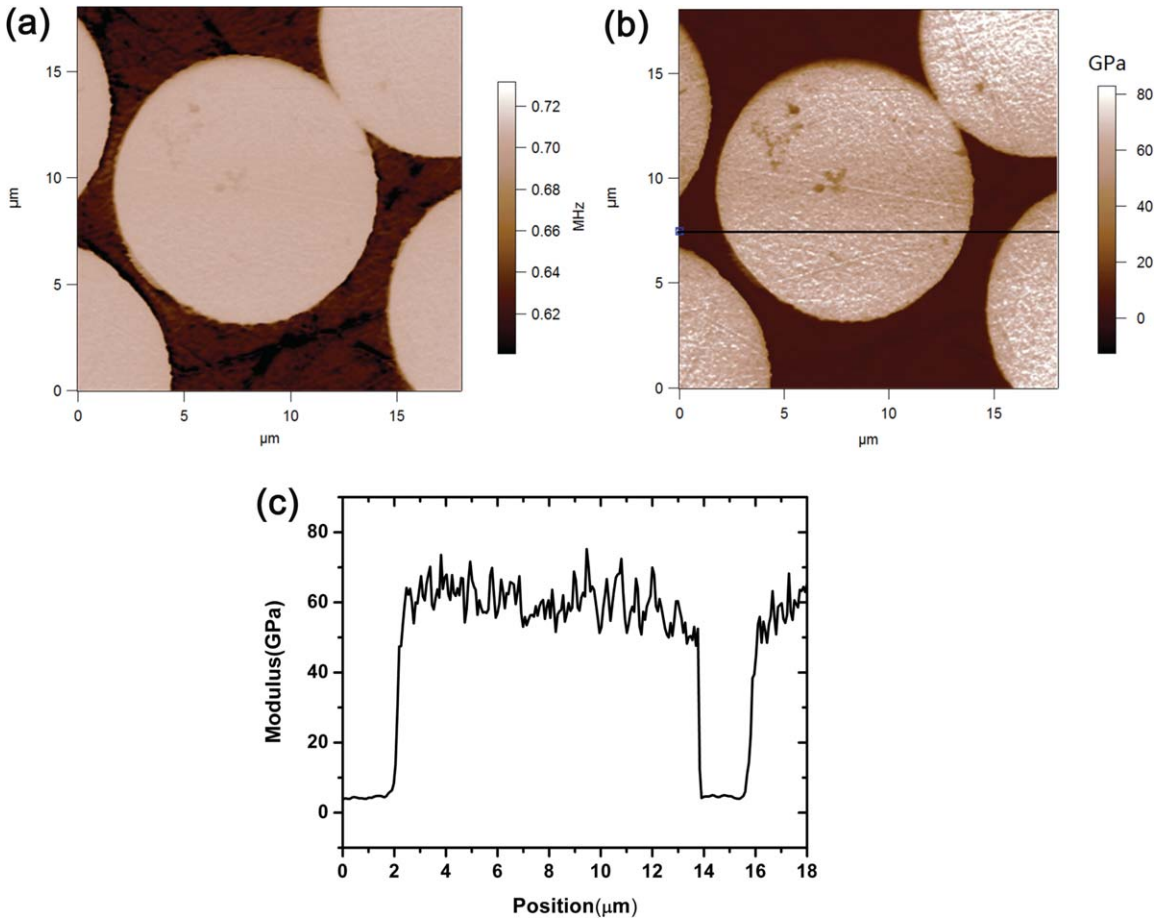

Figure 6. Quantitative modulus mapping of a GFRP using RT AFAM: (a) The CRF image, (b) the calculated indentation modulus image, and (c) the indentation modulus distribution of the line indicated in (b). [Color figure can be viewed in the online issue, which is available at wileyonlinelibrary.com.]

To test and verify the modulus mapping capacity of AFAM, we also conducted dynamic NI testing on this GFRP to make a comparison with AFAM. In dynamic NI testing, the static constant force is 2 μN, with the amplitude of the dynamic force of 1 μN and driven frequency of 250 Hz. The scan rate is 0.2 Hz, slow enough for instrument feedback during scanning. Meanwhile, to make the comparison more convincing, we conducted NI measurements at several locations and choose the modulus image with the smallest variations for comparison. Figure 7(a) is the measured storage modulus image of GFRP by dynamic NI. It can be seen that on the whole the fiber is stiffer than the epoxy, but the measured modulus in the fiber region is obviously not as uniform as that by AFAM [seen from Figure 6(c)]. Figure 7(b) is the modulus distribution of the line indicated part in Figure 7(a) (a line modulus distribution with the least fluctuation was selected), from which we calculated the storage modulus of the fiber is 99.53±34.23GPa with the relative error about 34.4% and that of the epoxy is 19.98±5.13GPa with the relative error about 25.7%. From Figures 6(b,c) and 7, it can be seen clearly that the relative errors for modulus measurement using AFAM is much smaller than that by dynamic NI, which may indicate some superiority of AFAM in nanoscale modulus mapping. Although in this case, AFAM showed more stable results, we could not simply conclude that modulus mapping function of CRFM is superior in measurement stability because AFAM can also be easily affected by the topography roughness. The reason why dynamic NI presented larger relative error in our experiments is probably because of that both the amplitude and phase of the indenter-sample system have to be simultaneously measured, and the phase response was much easily disturbed by other material's properties besides the mechanical property. Whereas for AFAM, the only measured quantity is the CRF of the tip-sample system. In addition, the modulus measurement results obtained by dynamic NI are much larger than the typical modulus values of the GFRP for both the epoxy (3–6 GPa) and the glass fiber (50–90 GPa). Despite the modulus difference from the typical value of glass fiber and the epoxy, the measured moduli by dynamic NI are stable and repeatable. These differences are probably because of that the NI indenter usually exerts a relatively large force to the sample surface and may introduce residual stress or plastic deformation in the sample after removing the indenter. The measurement accuracy of the next point may be affected by the adjacent created indentation by the indenter. Another reason may be that although the parameters of the instrument of NI were carefully calibrated before experiments, the tip shape function of the indenter may

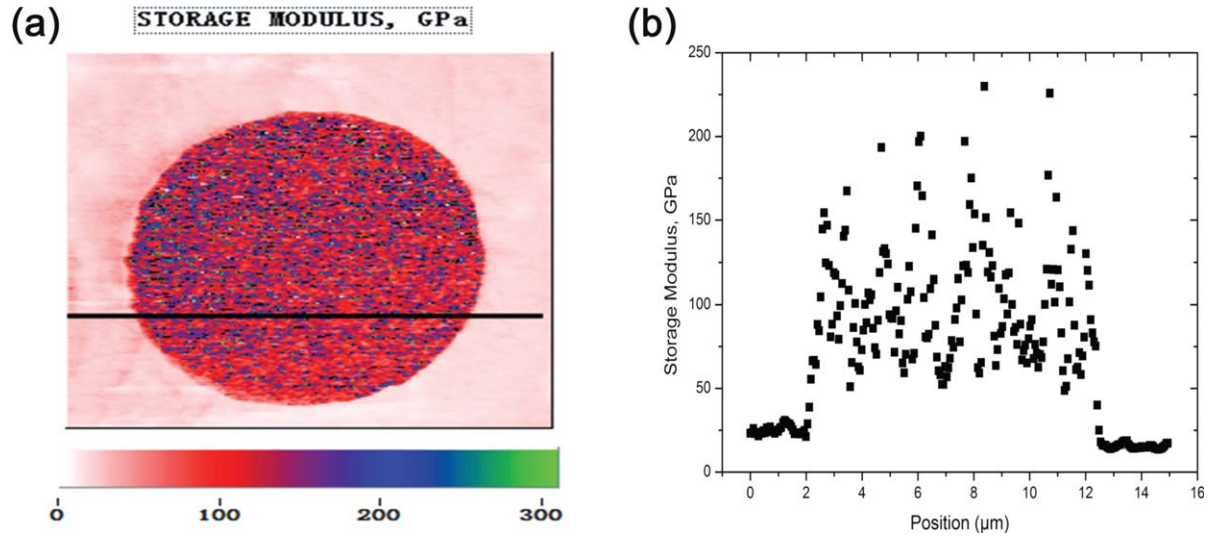

Figure 7. Modulus mapping images of a GFRP using dynamic NI: (a) the storage modulus and (b) the line scan modulus distribution indicated in (a). [Color figure can be viewed in the online issue, which is available at wileyonlinelibrary.com.]

not be so accurate during the penetration process.[5] So, it is recommended that combining both AFAM and NI may be a best choice to investigate the nanoscale mechanical property of materials.

High-Resolution Interface Characterization by AFAM

As the AFM cantilever has a small tip radius (5–50 nm) and the applying forces is also very small (from tens of nN to several μN), a high lateral resolution (typically about 10 nm) can be

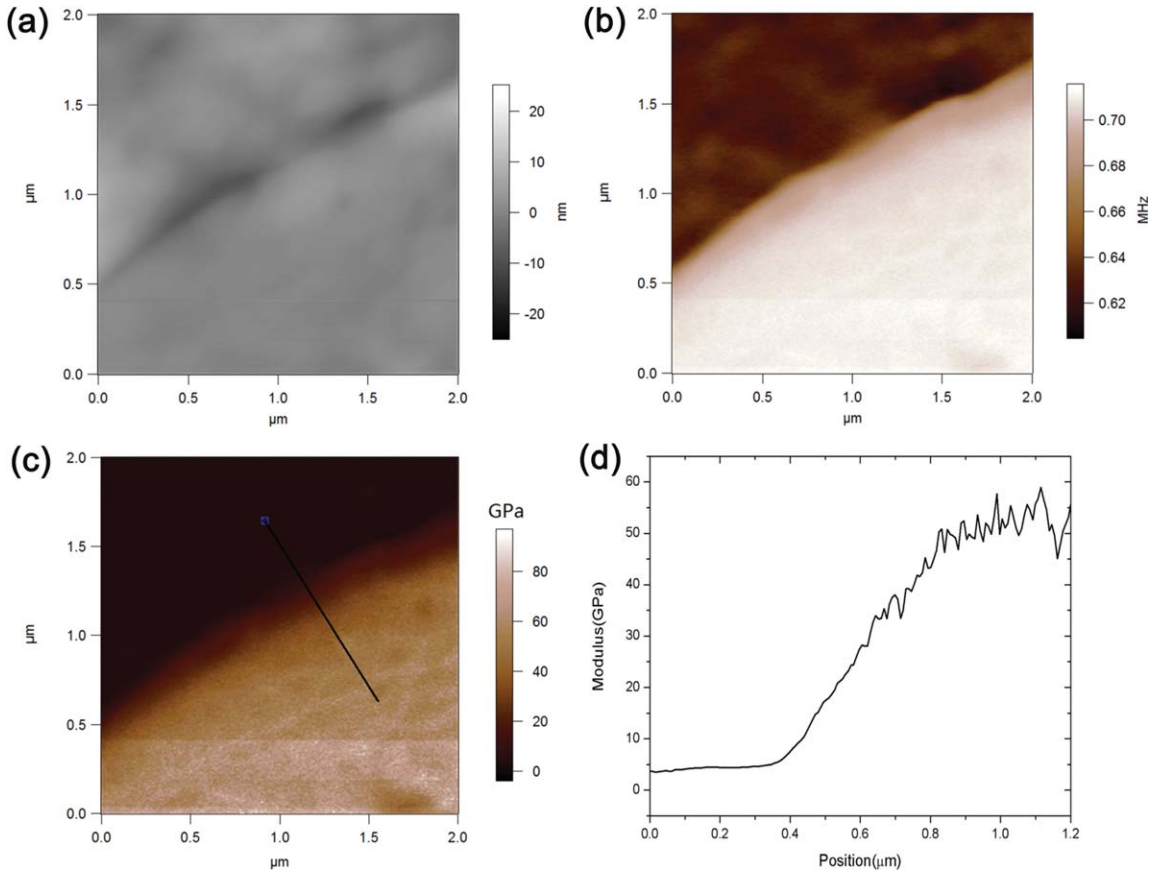

Figure 8. RT AFAM images of a GFRP near the interface region. (a) Topography, (b) the CRF image, (c) the calculated indentation modulus image, and (d) the modulus distribution of the indicated line in (c). [Color figure can be viewed in the online issue, which is available at wileyonlinelibrary.com.]

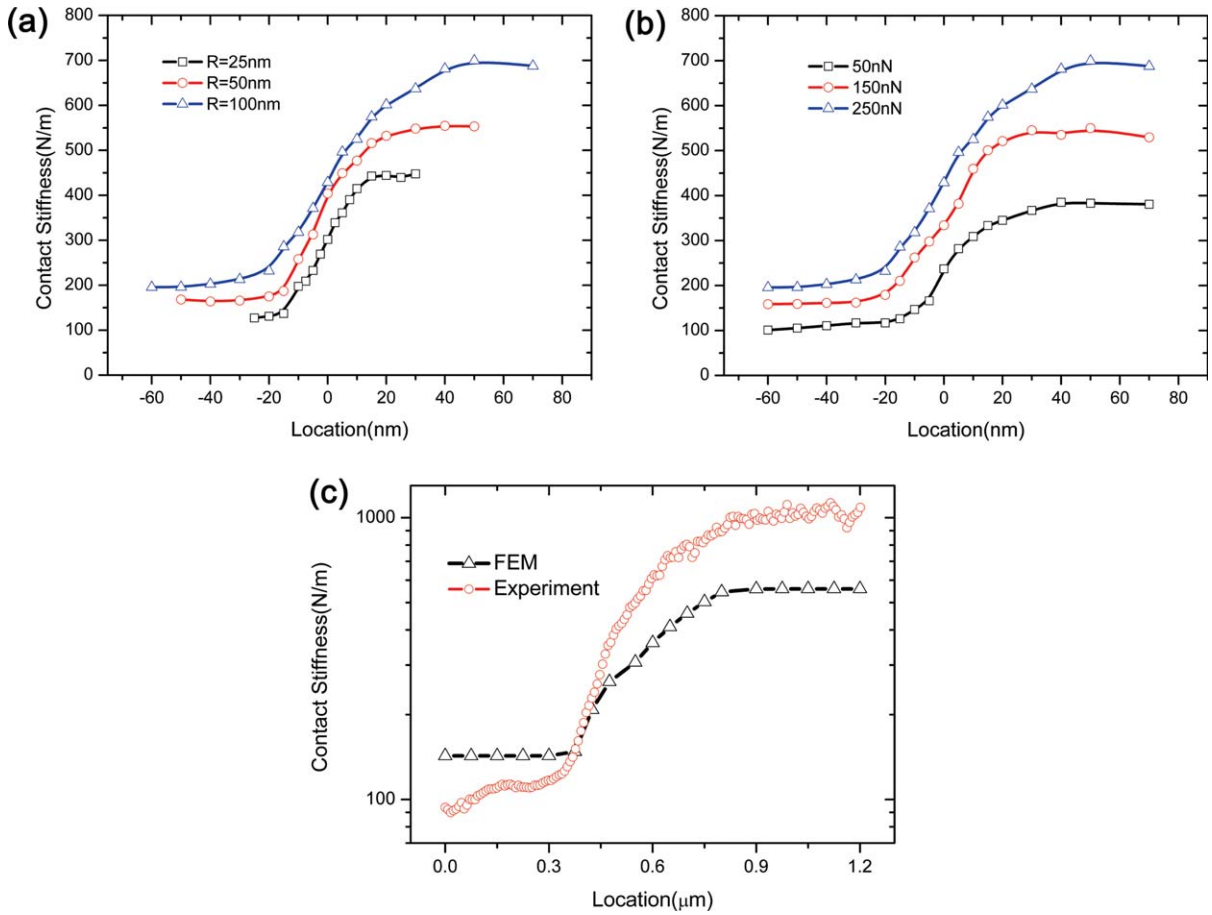

Figure 9. Finite element simulation results of contact stiffness variation across a sharp epoxy/fiber "interface" as well as a linear modulus variation interface with a finite interface width: (a) a sharp epoxy/fiber "interface" using different tip radii of 25, 50, and 100 nm, respectively, with the applied force of 250 nN; (b) a sharp epoxy/fiber "interface" using different applied forces of 50, 150, and 250 nN, respectively, with the tip radius of 100 nm; and (c) contact stiffness variation comparison between FEA of a linear-modulus-varied interface (with interface width 470 nm, tip radius 50 nm, and the applied force 250 nN) and AFAM measured experimental results. [Color figure can be viewed in the online issue, which is available at wileyonlinelibrary.com.]

obtained and AFAM can then present more accurate and reliable measurement of interface width, which is very difficult using other methods. In this work, a 2 μm $\times$ 2 μm mapping across the fiber/epoxy interface of the GFRP was conducted, as shown in Figure 8. It can be seen that the fiber/epoxy interface is clearly distinguished in the CRF image and the fiber is bonded very well with the epoxy. Also using a fused silica as the reference material, the indentation modulus image can be obtained based on the CRF image, as shown in Figure 8(c). A transition zone between the epoxy and the fiber can be clearly seen. A typical indentation modulus distribution across the interface is shown in Figure 8(d), from which we can clearly see that modulus increases gradually from the epoxy region to the fiber region and the transition zone between them is the interface.

To better understand the effect of tip radius and applied force on interface width measurement, FEA was specially implemented to investigate the contact stiffness variation across the interface. It is expected that when the cantilever tip scans in the epoxy region, approaching the interface, both the epoxy and interface region will have influences on the involved contact stiffness and thus the CRF. Similar case occurs when the tip scans in the fiber region and approaches the interface. Therefore, it is concluded that the measured interface width is always larger than its actual size. To simplify the analyzing process, the case of a sharp epoxy/fiber "interface" was first considered. Figure 9(a) is the simulated results of contact stiffness variation across the sharp "interface" with the applied force of 250 nN using different tip radii. Figure 9(b) shows the effect of applied force on the measured "interface" width. It can be seen that even for the sharp epoxy/fiber transition, a modulus transition zone or a "finite-width" interface still exists, which has not been taken into account in most interface measurements. As expected, the smaller the contact radius and the applied normal force, the smaller discrepancies between the real interface width and the measured value. A larger tip radius or applied force will inevitably lead to a larger testing error in the interface width measurement. Thus for interface characterization, a small pressing force as well as a small tip radius will give out more accurate values of the interface, which confirms that AFAM may be the most suitable method for interface characterization in composites, if the sample surface can be polished as flat as possible to reduce the roughness crosstalk.

To implement a more accurate interface width measurement, we adopted a lower limit (average modulus value of the epoxy plus the corresponding standard deviation, i.e. $(100\% + 15\%)M_{epoxy} = 115\%M_{epoxy}$) and an upper limit (average modulus value of the fiber minus the standard deviation, i.e. $(100\% - 10\%)M_{fiber} = 90\%M_{fiber}$) to determine the interface width. Based on the upper and lower limits of the modulus values, the average interface width is finally determined to be 476±45 nm with 10 randomly selected radial profiles across the interface, which is consistent with the previous measured values of between 100 nm and several μm.[4,5,15,16] Also to make similar comparison between the simulation and the experimental results, we conducted FEA simulations by setting an interface with linear-modulus-variation across the interface and the interface width to be 470 nm based on our experimental measurement. The comparison of the simulated contact stiffness variation across the interface by FEA and that by AFAM measurements is shown in Figure 9(c), from which we can clearly see that the contact stiffness transition width (about 525 nm) is still slight larger than the prescribed width of 470 nm. Note that there is a discrepancy between the specific measured contact stiffness values and the simulated contact stiffness values in Figure 9(c). This is probably because the measured contact stiffness is obtained based on the cantilever dynamics, whereas the finite element simulated contact stiffness is calculated based on contact mechanics. Other factors, for example the specific tip shape, tip radius, applied force and friction can also contribute to the discrepancy. Despite the above-mentioned discrepancies, the measured contact stiffness variation width based on both AFAM measurements and simulations are nearly the same. Bearing in mind the interface width is relatively large to the tip radius, in the case that the interface width is much smaller (<100 nm), the influence of the tip radius as well as the applied force will be more pronounced [Figure 9(a,b)], and AFAM will then be a more superior method for reliable and accurate interface measurements.

SUMMARY AND CONCLUSIONS

In summary, a DFRT technique was applied on AFAM and high-resolution and quantitative elastic modulus mapping of a GFRP was realized in this work. Using both the single-frequency AFAM and DFRT AFAM, the nanoscale mechanical properties of the GFRP were intensively characterized. Modulus mapping using dynamic NI was also conducted and compared with that by DFRT AFAM. Results show that DFRT AFAM is a reliable method for nanomechanical characterization. Interface characterization was specially performed on a 2 μm × 2 μm scanning area to show the high-resolution capability of AFAM. FEA was implemented to investigate the effect of tip radius as well as the applied force on interface measurement using a sharp "interface". Similar comparison between AFAM experimental results and FEA was also implemented by introducing a linear-modulus-varied interface with finite width in FEA. Finally, the interface width was determined to be 476 nm based on 10 random selected radial profiles across the interface.

Generally, AFAM is a powerful tool for nanomechanical property characterization of composites especially for the small scale interface. With the amplitude–frequency curve and phase–frequency curve at each pixel, quantitative viscoelasticity measurement can also be done for small damping materials.[34,35] But at present a fast and reliable viscoelasticity mapping method is still lacking. Besides, the influences of the surface roughness, tip wear during modulus imaging are still problems for AFAM which makes the accurate modulus measurement rather difficult. Better understanding of these issues will lead to refinement of AFAM for more accurate quantitative mechanical characterization of various materials.

ACKNOWLEDGMENTS

The authors gratefully thank the financial supports from the National Basic Research Program (973) of China under Grant No. 2011CB606105. Support from the National Natural Science Foundation of China (under Grant Nos. 11090331 and 11002002) is also acknowledged.

REFERENCES

1. Bansemir, H.; Haider, O. *Cryogenics* **1998**, *38*, 51.
2. Hollaway, L. C. *Constr. Build. Mater.* **2003**, *17*, 365.
3. McConnell, V. P. Comprehensive Composite Materials; Elsevier: Amsterdam, **2000**.
4. Nair, S. S.; Wang, S. Q.; Hurley, D. C. *Compos. Part A: Appl. Sci. Manuf.* **2010**, *41*, 624.
5. Gu, Y. Z.; Li, M.; Wang, J.; Zhang, Z. G. *Carbon* **2010**, *48*, 3229.
6. Zhao, W.; Singh, R. P.; Korach, C. S. *Compos. Part A: Appl. Sci. Manuf.* **2009**, *40*, 675.
7. Joseph, P. V.; Rabello, M. S.; Mattoso, L. H. C.; Joseph, K.; Thomas, S. *Compos. Sci. Technol.* **2002**, *62*, 1357.
8. Hodzic, A.; Kim, J. K.; Lowe, A. E.; Stachurski, Z. H. *Compos. Sci. Technol.* **2004**, *64*, 2185.
9. Kim, J. K.; Mai, Y. W. Engineered Interfaces in Fiber Reinforced Composites; Elsevier: New York, **1998**.
10. Drzal, L. T. *Adv. Polym. Sci.* **1986**, *75*, 1.
11. DiBenedetto, A. T. *Mater. Sci. Eng. A* **2001**, *302*, 74.
12. Piggott, M. R. *Mater. Res. Soc. Symp.* **1990**, *170*, 265.
13. Hodzic, A.; Stachurski, Z. H.; Kim, J. K. *Polymer* **2000**, *41*, 6895.
14. Wang, H. F.; Nelson, J. C.; Gerberich, W. W.; Deve, H. E. *Acta Metall. Mater.* **1994**, *42*, 695.
15. Kim, J. K.; Sham, M. L.; Wu, J. S. *Compos. Part A: Appl. Sci. Manuf.* **2001**, *32*, 607.
16. Gao, S. L.; Mader, E. *Compos. Part A: Appl. Sci. Manuf.* **2002**, *33*, 559.
17. Appiah, K. A.; Wang, Z. L.; Lackey, W. J. *Carbon* **2000**, *38*, 831.
18. Montes-Morán, M. A.; Young, R. J. *Carbon* **2002**, *40*, 857.
19. Song, Y. X.; Bhushan, B. *J. Phys.: Condens. Matter* **2008**, *20*, 225012.
20. Rabe, U. In Applied Scanning Probe Methods II; Bushan, B., Fuchs, H., Eds.; Springer-Verlag: Berlin, **2006**; p 37.

21. Hurley, D. C. In Applied Scanning Probe Methods XI; Bushan, B.; Fuchs, H., Eds.; Springer: Berlin, **2009**; p 97.
22. Rabe, U.; Amelio, S.; Kopycinska, M.; Hirsekorn, S.; Kempf, M.; Goken, M.; Arnold, W. *Surf. Interface Anal.* **2002**, *33*, 65.
23. Hurley, D. C.; Kopycinska-Muller, M.; Kos, A. B.; Geiss, R. H. *Meas. Sci. Technol.* **2005**, *16*, 2167.
24. Kos, A. B.; Hurley, D. C. *Meas. Sci. Technol.* **2008**, *19*, 015504.
25. Rodriguez, B. J.; Callahan, C.; Kalinin, S. V.; Proksch, R. *Nanotechnology* **2007**, *18*, 475504.
26. Xie, S. H.; Gannepalli, A.; Chen, Q. N.; Liu, Y. M.; Zhou, Y. C.; Proksch, R.; Li, J. Y. *Nanoscale* **2012**, *4*, 408.
27. Gannepalli, A.; Yablon, D. G.; Tsou, A. H.; Proksch, R. *Nanotechnology* **2011**, *22*, 355705.
28. Johnson, K. L. Contact Mechanics; Cambridge University Press: Cambridge, **1985**.
29. Hutter, J. L.; Bechhoefer, J. *Rev. Sci. Instrum.* **1993**, *64*, 1868.
30. Asif, S. A. S.; Wahl, K. J.; Colton, R. J.; Warren, O. L. *J. Appl. Phys.* **2001**, *90*, 1192.
31. Killgore, J. P.; Kelly, J. Y.; Stafford, C. M.; Fasolka, M. J.; Hurley, D. C. *Nanotechnology* **2011**, *22*, 175706.
32. Hurley, D. C.; Kopycinska-Müller, M.; Kos, A. B.; Geiss, R. H. *Adv. Eng. Mater.* **2005**, *7*, 713.
33. Jesse, S.; Baddorf, A. P.; Kalinin, S. V. *Nanotechnology* **2006**, *17*, 1615.
34. Hurley, D. C. In Scanning Probe Microscopy of Functional Materials: Nanoscale Imaging and Spectroscopy; Kalinin, S. V., Gruverman, A., Eds.; Springer Science+Business Media, LLC: New York, **2010**; p 95.
35. Killgore, J. P.; Yablon, D. G.; Tsou, A. H.; Gannepalli, A.; Yuya, P. A.; Turner, J. A.; Proksch, R.; Hurley, D. C. *Langmuir* **2011**, *27*, 13983.